Smart Structures and Systems, *Vol. 25, No. 1 (2020) 23-35*
DOI: https://doi.org/10.12989/sss.2020.25.1.023

Temperature analysis of a long-span suspension bridge based on a time-varying solar radiation model

Qi Xia [1,2], Senlin Liu [1,2] and Jian Zhang*[1,2]

[1] *Jiangsu Key Laboratory of Engineering Mechanics, Southeast University, 210096, Nanjing, China*
[2] *School of Civil Engineering, Southeast University, 210096, Nanjing, China*

(*Received August 21, 2018, Revised September 23, 2019, Accepted September 28, 2019*)

Abstract. It is important to take into account the thermal behavior in assessing the structural condition of bridges. An effective method of studying the temperature effect of long-span bridges is numerical simulation based on the solar radiation models. This study aims to develop a time-varying solar radiation model which can consider the real-time weather changes, such as a cloud cover. A statistical analysis of the long-term monitoring data is first performed, especially on the temperature data between the south and north anchors of the bridge, to confirm that temperature difference can be used to describe real-time weather changes. Second, a defect in the traditional solar radiation model is detected in the temperature field simulation, whereby the value of the turbidity coefficient t_u is subjective and cannot be used to describe the weather changes in real-time. Therefore, a new solar radiation model with modified turbidity coefficient γ is first established on the temperature difference between the south and north anchors. Third, the temperature data of several days are selected for model validation, with the results showing that the simulated temperature distribution is in good agreement with the measured temperature, while the calculated results by the traditional model had minor errors because the turbidity coefficient t_u is uncertainty. In addition, the vertical and transverse temperature gradient of a typical cross-section and the temperature distribution of the tower are also studied.

Keywords: solar radiation; turbidity coefficient; heat-transfer analysis; temperature distribution; structural health monitoring

1. Introduction

Bridges are subject to varying environmental thermal effects, with the temperature load having a significant influence on the bridge static/dynamic responses. The thermal behavior of long-span bridges exhibits a complex dependence on the air temperature, solar radiation, wind, as well as the material and structure types. Considerable efforts have previously been devoted to the investigation of the temperature distribution and thermal effects on the long-span bridges (Xu *et al*. 2010, Zhou and Yi 2013, Zhou *et al*. 2015, Chen *et al*. 2017, Kim *et al*. 2017, Xia *et al*. 2017a, Yang *et al*. 2017, Abid *et al*. 2018).

The rapid developments of numerical analysis and computer-processing capacity have made it possible to perform extensive studies on the temperature behavior of various types of bridges for which a solar radiation model has been developed (Dilger *et al*. 1983, Tong *et al*. 2001). Kim *et al*. (2009) proposed a method to predict the three-dimensional (3D) temperature distribution of curved steel box-girder bridges using the energy equation for solar radiation. Xia *et al*. (2013) investigated the effects of heat flow on a long-span suspension bridge through the analysis of 3D numerical simulations, with the results compared with the on-site monitoring data.

*Corresponding author, Professor,
E-mail: jian@seu.edu.cn

Transient thermal response mechanisms are depended upon the input parameters, especially the solar radiation density, which results in structural temperature variations with time and location. For example, the turbidity coefficient is an important parameter in the solar radiation model, which accounts for the effect of clouds and air pollution. For clear sky (e.g., cloudless weather), the turbidity coefficient varies between 1.8 and 3; for a heavy industrial environment, the coefficient may be as high as 8 or 9 (Elbadry and Ghali 1983). However, the turbidity coefficient may take a range of values, with no uniform rules for its evaluation. In most thermal performance studies and solar radiation calculations, the turbidity coefficient has always been considered a time-invariant value in the thermal analysis process (Liu *et al*. 2012, Chen *et al*. 2013, Song *et al*. 2016, Wang *et al*. 2016)

While the turbidity coefficient has not been studied throughly in the past, nonetheless it significantly affects the amount of direct solar radiation to the surface of the bridge deck. Westgate *et al*. (2015) considered the important role that cloud cover plays on the levels of solar radiation intensity and estimated the solar radiation indirectly using the temperature difference between the suspension cable and truss. Zhou *et al*. (2016) constructed a two-dimensional finite-element model of a box girder to study the thermal performance of a long-span suspension bridge. The turbidity coefficient in the daytime was determined based on the cloud cover obtained from meteorological measurements. Therefore, while these investigations are

http://www.techno-press.org/?journal=sss&subpage=7
ISSN: 1738-1584 (Print), 1738-1991 (Online)

very meaningful for the determination of the exact solar radiation density, there is still a need to consider the turbidity coefficient as a time-varying parameter throughout the day, where the turbidity coefficient has been previously set to a time-invariant value. However, as the weather conditions are subject to real-time changes, this implies a varying turbidity coefficient throughout the day.

Our objective is to develop a time-varying turbidity coefficient and solar radiation model, and used to study the temperature distribution and characteristics of a typical section of a long-span bridge. First, the studied bridge and its structural health monitoring (SHM) system are described briefly. The temperature data of the south and the north anchors are compared and analyzed under different environmental conditions. Second, the time-varying turbidity coefficient and modified solar-radiation model are established based on the temperature difference between the south and north anchors. The results of temperature simulations of a typical cross-section are compared for different turbidity coefficients. Third, the vertical and transversal temperature distributions of the box girder are also investigated, including the calculation of the temperature variations of the tower section. Finally, the conclusions are provided.

2. Details of the studied bridge and data analysis

2.1 The Jiangyin Bridge and its SHM system

The Jiangyin suspension bridge with a main span length of 1,385 m over the Yangtze River in Jiangsu, China as shown in Fig. 1(a). The main span has a welded streamlined constant depth steel box girder of 3 m height and 36.9 m width utilizing the asphalt concrete pavement, and a navigation clearance of 50 m. The bridge has two reinforced concrete towers of 190 m height, with the main cables are anchored in gravity anchorages. The air temperature changes from -6.1°C to 37.2°C throughout the year, with an annual average temperature of about 16.9°C.

The SHM system was designed and installed on the bridge in 2005 (Ko and Ni 2005, Xia *et al*. 2017b), with the current system including about 170 sensors, such as accelerometers, fiber bragg grating sensors (FBG), displacement sensors, global positioning system receivers, shear pins, and ultrasonic anemometers, etc. For a long-span suspension bridge, the temperature field of the structure is extremely complex and requires many components to be monitored. First, two meteorological sensors (MS) are arranged on the south and north anchors of the bridge. Second, nine equidistant cross sections of the main span are fitted temperature measurements as shown in Fig. 1(b). In each section, eight FGB strain (FBGS) and four FBG temperature (FBGT) sensors are installed on each cross section to measure strain and temperature, respectively. Here, the monitoring data of the second year of the installation of the SHM system in 2006 is used to investigate the temperature distribution and solar radiation.

2.2 Meteorological data analysis

The ambient temperature (air temperature) is the boundary condition of the bridge structure for convective heat transfer. Two meteorological sensors have been deployed in the SHM system of the studied bridge to monitor the local atmospheric temperature, which are located on the south and north anchors respectively as shown in Fig. 2.

Meteorological sensor 1 (MS1) is located at the entrance of the north anchor and is used to collect air temperature and humidity data as shown in Fig. 2(a). It should be noted that while MS1 is installed in a metal box to protect it from

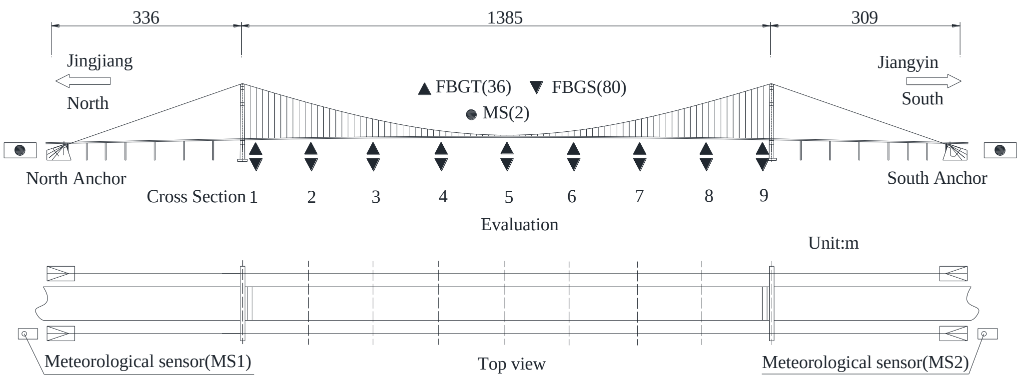

(a) Partial sensor layout

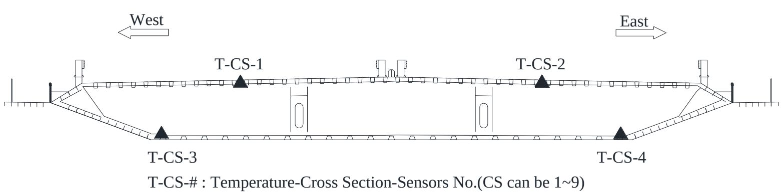

(b) Temperature sensor arrangement on cross section

Fig. 1 SHM system of studied bridge

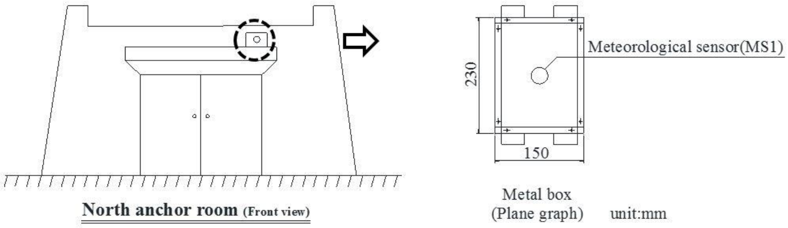

(a) MS1 located on north anchor

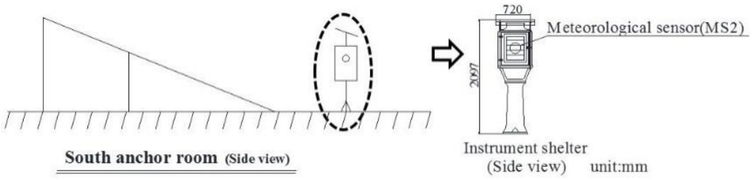

(b) MS2 located on south anchor

Fig. 2 Layout of meteorological sensors

disturbances, such as wind, rain, snow, etc. and the metal box is exposed to direct sunlight. Therefore, for direct sunlight on the metal box, the measured temperature not only contains the atmospheric temperature, but also an additional temperature contribution from solar radiation.

Meteorological sensor 2 (MS2) is located above the platform of the south anchor as shown in Fig. 2(b) and is installed in a shelter to isolate it form solar radiation, and protect against strong winds, rain, snow and other effects, giving a more accurate reading of the outside air temperature and humidity changes.

Analyses of monitoring data are as follows. Fig. 3(a) shows temperature monitoring data for MS1 and MS2 in February 2006. The temperature data at north anchor are indicated by a curve with circles; the temperature data at south anchor are represented by a curve with asterisks. The temperature at south anchor reaches a maximum of 17.9°C and a minimum of -5.4°C. The temperature at north anchor reaches a maximum of 25.8°C and a minimum of-4.6°C. Fig. 3(b) shows the temperature data for MS1 and MS2 on a sunny day (clear sky), where it is observed that the temperature from north anchor is significantly greater than that at south anchor, while at night, the temperatures at both anchors are almost the same. Fig. 3(c) shows the temperature data for MS1 and MS2 on a cloudy day, where the temperature of north anchor is consistent with the temperature of south anchor throughout the day. The reason for this phenomenon is that the temperature measured at south anchor reflects the air temperature, and the temperature of north anchor reflects both the air temperature and the additional heating from the solar radiation. When the weather is completely cloudy, the temperature of north anchor is the same as the temperature of south anchor, and the effects of solar radiation are not obvious.

Fig. 4(a) shows the temperature monitoring data for MS1 and MS2 in May 2006. The temperature at south anchor reaches a maximum of 32.3°C and a minimum of

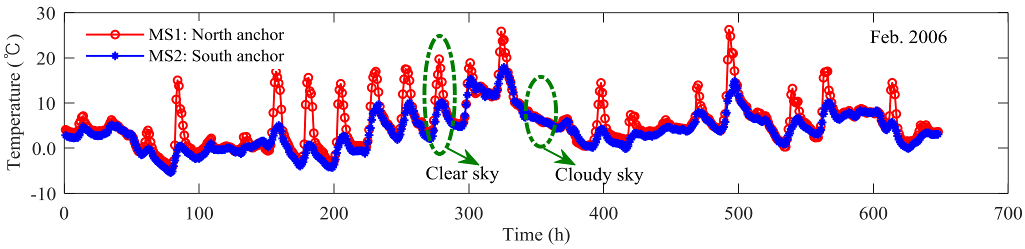

(a) Temperature variation data

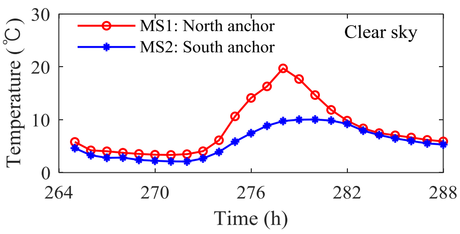

(b) Clear sky

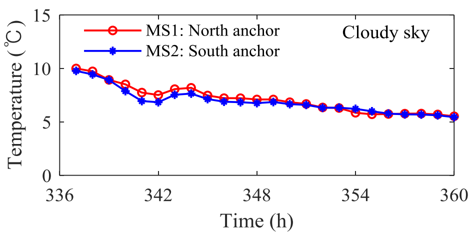

(c) Cloudy sky

Fig. 3 Temperature variations of the north and south anchors in Feb 2006

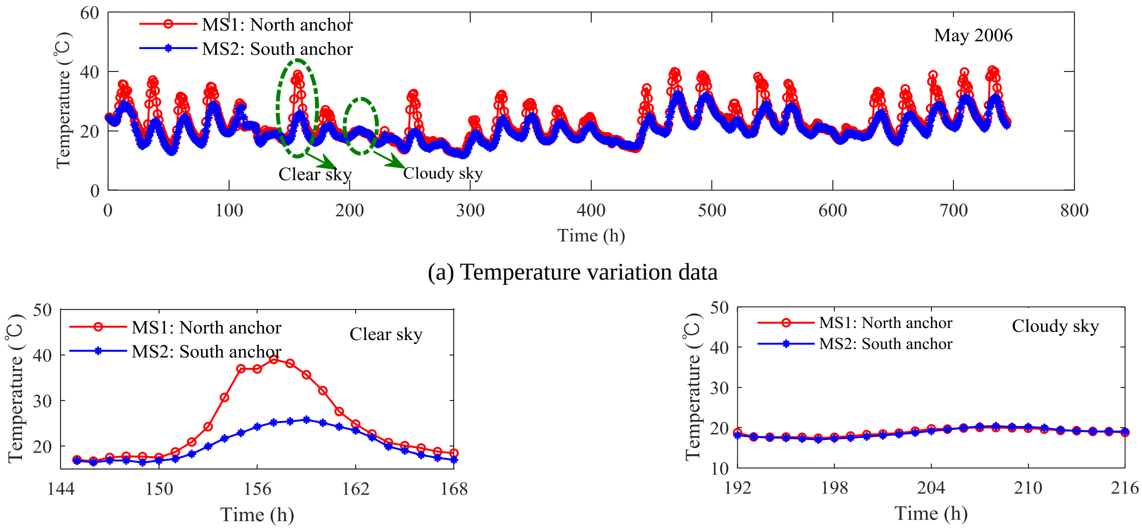

(a) Temperature variation data

(b) Clear sky

(c) Cloudy sky

Fig. 4 Temperature variations of the north and south anchors in May 2006

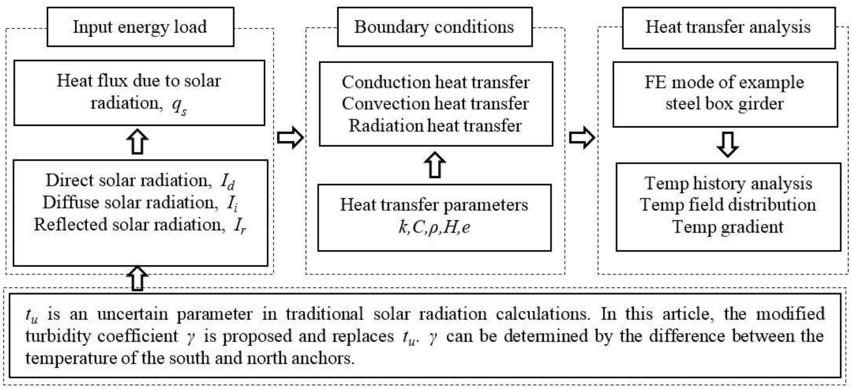

Fig. 5 Flowchart of calculating solar energy and predicting temperature distribution

11.9°C. The temperature at north anchor reaches a maximum of 39.8°C and a minimum of 12.5°C. Figs. 4(b)-(c) show the comparison of temperature monitoring data on sunny and cloudy days, respectively, where phenomena are consistent with Figs. 3(b)-(c).

Based on the above sensor installation and measurement data analysis, the following conclusions can be drawn: (1) the temperature difference between the north and south anchors is caused by solar radiation; (2) the temperature difference between the north and south anchors reflects the weather conditions in real-time. These conclusions will be used to modify the traditional turbidity coefficient (t_u) in Section 3 and to accurately determine the solar radiation density.

2.3 Proposed improvements in temperature field simulation

When temperature fields of the structures are accurately simulated, techniques not only need a precise finite element model (FEM), but also require reliable external load data, especially the solar radiation density, which is the primary cause of structural temperature increase. The fine FEM can be established based on the model updating method by using monitoring data, but the load data of solar radiation density can only be calculated by theories in the case of limited radiometers. Therefore, the rough load data will eventually lead to inaccuracies or errors in the temperature field simulation (Zhang *et al*. 2013).

The study found the reason for this phenomenon is that the parameter of turbidity coefficient t_u is difficult to estimate (Dilger *et al*. 1983, Elbadry and Ghali 1983), and subject to local climatic interaction. For example, one literature (Zhu and Meng 2017) consider it as a constant in the temperature simulation. This article will establish a time-varying parameter γ to replace t_u, using the temperature difference between the south and north anchors. The simulation process of temperature field and the contribution of this article are shown in Fig. 5.

3. Solar radiation effects

3.1 Solar radiation model and its components

The temperature at any point within the structure at any time is estimated by applying established principles of heat transfer as illustrated in Fig. 6. The structure temperature is

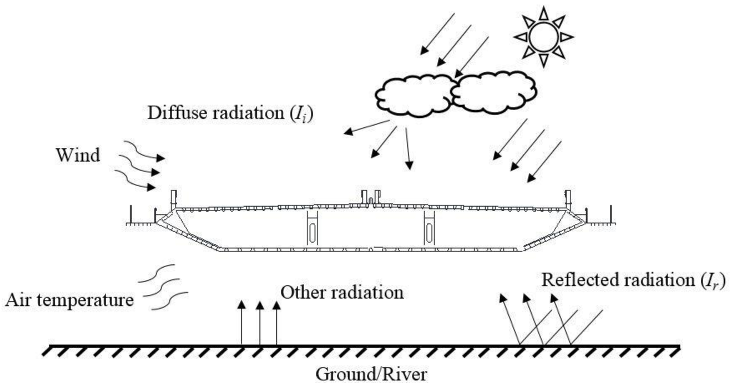

Fig. 6 Thermal environments of a bridge girder

affected by: (1) heat transfer by conduction within the material; (2) heat generated within the material; (3) heat transfer at the surface of the structure by convection; (4) the radiant heat flux at the boundary of the element.

The rate of heat absorbed by the surfaces of a bridge structure due to solar radiation q_s is (Rohsenow *et al*. 1998)

$$\boldsymbol{q_s = \alpha I} \tag{1}$$

where α ($0 < \alpha < 1$) is absorptivity coefficient of the surface material and I is solar radiation (Branco and Mendes 1993)

$$I = I_d + I_i + I_r \tag{2}$$

in which, I_d is direct solar radiation, I_i is diffuse solar radiation, and I_r is reflected solar radiation on a surface.

The direct solar energy to heat up the bridge structure depends on the solar constant I_{sc} and the absorption of the solar energy in the atmosphere. The Earth's atmosphere acts as a filter for the solar radiation so that only a fraction of the total solar radiation reaches the surface of the Earth, which can be expressed by (Elbadry and Ghali 1983, Branco and Mendes 1993)

$$I_n = I_{sc} K_T \tag{3}$$

where I_{sc} is the solar insolation on a plane at the outer edge of the Earth's atmosphere, is denoted as the solar constant 1367±7W/m^2. Here, K_T is a transmission coefficient accounting for the attenuation of solar radiation by the atmosphere (Elbadry and Ghali 1983)

$$K_T = 0.9^{\frac{k_a t_u}{sin(\theta_a + 5°)}} \tag{4}$$

where k_a is the ratio of atmospheric pressure to the pressure at sea level, t_u is a turbidity factor accounting for the effect of clouds and air pollution, and θ_a is the solar altitude.

The presence of air pollution increases substantially the absorption of the solar radiation for which the turbidity factor t_u is used to express the attenuation of the radiation in different atmospheric conditions. For clear skies, the turbidity factor varies between 1.8 and 3, while for a heavy industrial environment, this factor may be as high as 8 or 9. In most calculations, the value t_u is held constant throughout the day.

Radiation intensity on structural surfaces after atmospheric attenuation can be expressed as

$$I_d = I_n \cos\theta \tag{5}$$

where θ is solar incident angle.

Diffuse sky radiation is the portion of solar radiation energy reaching the Earth's surface after being scattered by the atmosphere. Diffuse radiation on structure surfaces depends on the solar altitude angle and the atmospheric transparency coefficient, but is not contingent on the azimuth of the surface. The energy reaching the earth's surface by diffuse solar radiation can be estimated (Li 1996)

$$I_{iH} = (0.271 I_{sc} - 0.294 I_n) sin\beta_s \tag{6}$$

where β_s is the solar altitude. Sky scattering intensity on an inclined plane can be expressed as (Li 1996)

$$I_i = I_{iH} \frac{1 + sin\,\beta_b}{2} \tag{7}$$

where β_b is angle between the normal to the inclined plane and horizontal plane.

Ground-reflected radiation absorbed by an inclined plane can be calculated (Li 1996).

$$I_r = \rho^* (I_n + I_i)(1 - cos\,\beta_b)/2 \tag{8}$$

where ρ^* is the reflected coefficient of ground.

3.2 Heat transfer

Conduction Heat Transfer. Heat transfer by conduction in the z-direction is described by one-dimensional Fourier's equation (Rohsenow *et al*. 1998)

$$C \frac{\partial T}{\partial t} = \frac{k}{\rho} \frac{\partial^2 T}{\partial z^2} + \frac{q_v}{\rho} \tag{9}$$

where k is the thermal conductivity, C is specific heat capacity, ρ is the density, and q_v is the rate of heat generation within the body.

Convection Heat Transfer. The rate of heat transfer

(Elbadry and Ghali 1983) by convection is related to the temperature difference between the surface temperature T_s, and the air temperature T_a

$$q_c = H(T_s - T_a) \tag{10}$$

where H is convective heat transfer coefficient.

Radiation Heat Transfer. The exchange of heat by radiation, q_r between two bodies at temperature T_{s1} and T_{s2} is expressed by (Threlkeld 1970)

$$q_r = eC_s[T_{s1}^4 - T_{s2}^4] \tag{11}$$

where e is the emissivity of the surface $(0 < e < 1)$, and C_s is the Stefan-Boltzmann constant.

3.3 Modified on turbidity coefficient

The coefficient t_u is a turbidity factor accounting for the effect of clouds and air pollution. Cloud cover has not been well studied in the bridge community, but it affects the amount of solar radiation the surface of the bridge deck receives directly. The value of t_u only depends on small and inaccurate meteorological data. Therefore, the proposed modified turbidity coefficient γ is established on real-time monitoring data and replaces the coefficient t_u. The theoretical derivations are as follows:

The range of traditional turbidity coefficient t_u is expressed

$$t_u = \begin{cases} 1.8\sim3 & \text{(Clear sky)} \\ 3\sim8 & \\ 8\sim9 & \text{(Cloudy sky)} \end{cases} \tag{12}$$

When $t_u = 1.8\sim3$, show that the weather is good (clear sky). When $t_u = 8\sim9$, show that the weather is bad (complete cloudy, a heavy industrial environment). When $t_u = 3\sim8$, the weather conditions indicate between clear sky and cloudy sky and are not easy to determine.

The values of turbidity coefficient in some literatures are shown in the Fig. 7. Turbidity coefficients of 2, 1.8, 3.5, 3.25, 4.2 are taken from the literatures of Dilger *et al*. (1983), Elbadry and Ghali (1983), Niu *et al* (2014), Tian *et al*. (2017) respectively. Most scholars have given turbidity coefficients under sunny day, because of the temperature effects of structures are very significant under this weather condition. This has also led to very few studies on extreme weather conditions, giving rise to more uncertainty in the value of turbidity coefficient.

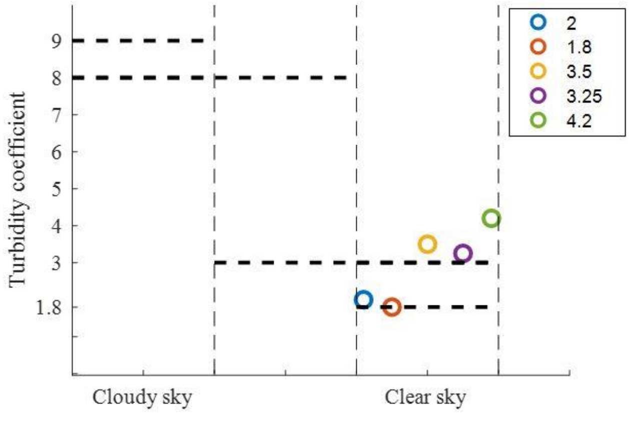

Fig. 7 The values of turbidity coefficient

From the section 2, the conclusion is that the temperature difference between the north and south anchors can reflects the weather conditions. The formulas are expressed as followed

$$T_n = T_a + \Delta T \tag{13}$$

$$T_a = T_s \tag{14}$$

$$\Delta T = T_n - T_s \tag{15}$$

where T_n is the temperature at north anchor, T_s is the temperature at south anchor, T_a is air temperature, and ΔT is the difference between the temperature of north and south anchors. When $\Delta T > 0$, that is indicates the weather is good (clear sky). When $\Delta T = 0$, that is means the weather is bad (completely cloudy). Therefore, the temperature difference can describe the weather changes in real-time. Then, the range of temperature difference ΔT in the whole year is first acquired.

A statistical analysis of the temperature difference ΔT between north and south anchors in 2006 is performed, assuming that the temperature does not change much over one hour, which allows the analysis of one-hour averages of the monitoring data. The histogram of the temperature difference ΔT is shown in Fig. 8 and the range of ΔT is about 0°C~20°C.

The literatures (Westgate *et al*. 2015, Zhou *et al*. 2016) studied the difference between the temperature of the suspension cable and truss, which was used to approximate the cloud cover levels. Therefore, this assumption is also adopted to determine the turbidity coefficient in this article. A modified turbidity coefficient γ is proposed and expressed

$$\gamma = -\frac{7.2}{20}\Delta T_t + 9 \tag{16}$$

where γ is the modified turbidity coefficient and replaces t_u, and ΔT_t is a real-time temperature difference between the north and south anchors. When $\Delta T_t = 0$, it means that the sky is totally covered in cloud ($\gamma = 9$). When $\Delta T_t = 20$, and it means that the sky is completely cloudless ($\gamma = 1.8$). The comparison between t_u and γ is shown in Table 1.

The coefficients of t_u and γ are compared in Fig. 9 with the days of Feb 17, 2006 and Jun 13, 2006. X axis indicates the daytime, the sunrise is 6 am, and the sunset is 18 pm. Y axis indicates turbidity coefficients. From the Fig. 9, the dashed lines represent the traditional turbidity coefficients (t_u), which are constant during a day; and the solid lines represent the modified turbidity coefficients (γ), which change in real-time. Obviously, if original coefficients are adopted, the calculated values of solar radiation density are inaccurate. Modified turbidity

Table 1 The comparison between t_u and γ

Atmospheric condition	Before modified	After modified	Temperature difference
	t_u	$\gamma = -0.36\Delta T_t + 9$	ΔT_t
Clear sky (completely cloudless)	1.8~3	1.8~3.02	20°C ~16.6°C
Cloudy sky	uncertainly	3.02~8.02	16.6°C ~2.7°C
Cloudy sky (totally covered in cloud)	8~9	8.02~9	2.7°C ~0°C

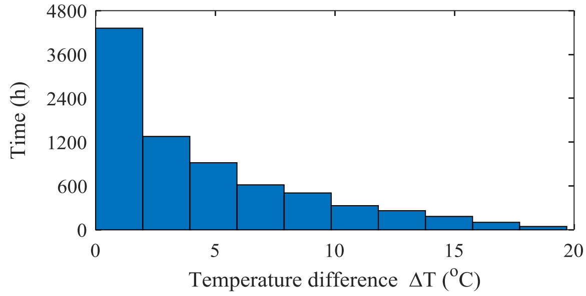

Fig. 8 The histogram of the temperature difference between the north and south anchors in 2006

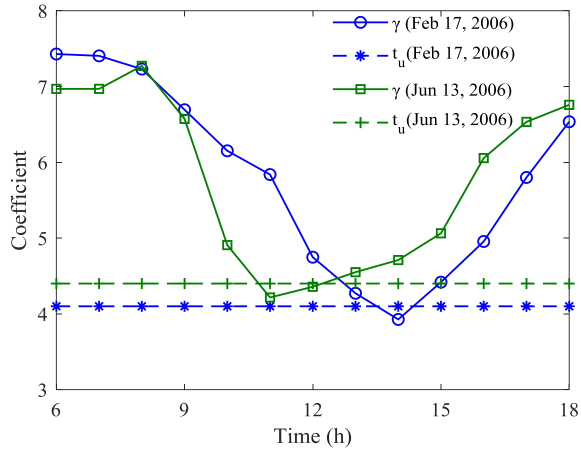

Fig. 9 Comparison of t_u and γ throughout the day of Feb 17 and Jun 13, 2006

coefficients are more realistic and can accurately determine the solar radiation density.

4. Thermal analysis of box girder

4.1 FEM and thermal parameters

The 3D FEM of the Jiangyin suspension bridge is developed from a combination of shell and line elements by using ANSYS 15 software, as shown in Fig. 10. The main cables, hangers, and towers are modeled using link33 and

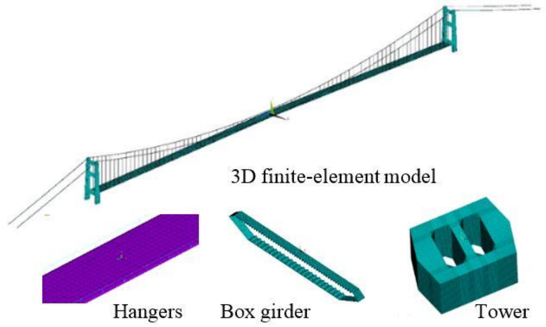

Fig. 10 3D FEM of the studied bridge and local details

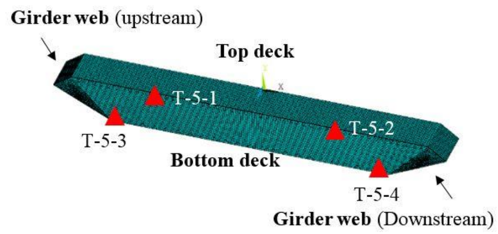

Fig. 11 Finite element of a typical cross section at mid-span

Table 2 Material parameters for thermal analysis

Parameters	Asphalt	Steel	Concrete
k, Heat transfer (W/(m℃))	1.01	48	1.54
ρ, Density(kg/m^3)	2360	7850	2600
C, Specific heat (J/kg℃)	1680	480	950
Absorptivity coefficient	0.90	0.685	0.65
Emissivity coefficient	0.90	0.8	0.8

Table 3 Geography parameters for a typical cross section

Parameters	Value
ϕ, Latitude	31.94°
δ, Solar declination angle	$23.45\sin\left(360\frac{284+N}{365}\right)$, N is number of days
γ, Surface azimuth angle (web)	114.4° (downstream), -65.5° (upstream)
β, dip angle (web)	32.48° (downstream), 32.48° (upstream)
τ, hour angle	15×(12-i), i = 6, 7, 8…18
I_{sc} , solar constant	1367 w/m^2
k_a , Atmospheric relative pressure	1

the steel-box girder are constructed using the elastic shell 63 elements. The entire FEM consists of 37276 nodes and 23070 elements.

The thermal boundary conditions are calculated and applied to the FEM for a transient heat-transfer analysis. The numerical model of a typical cross section at mid-span is shown in Fig. 11. T-5-1 and T-5-3 will selected as the measured values to compare with the simulation results. Finally, the main material and geography parameters are summarized in Tables 2 and 3.

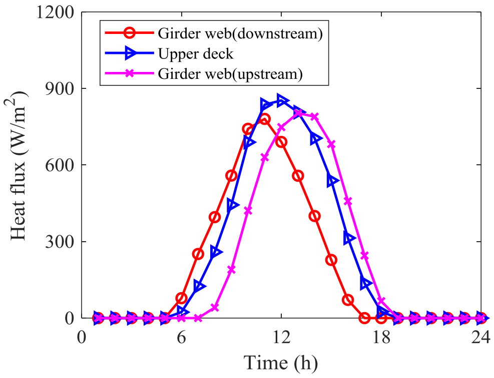

Fig. 12 Solar radiation intensity on June 13, 2006

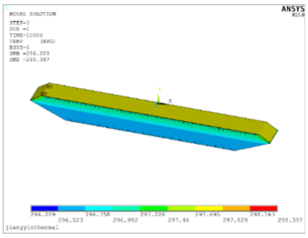
(a) 3:00

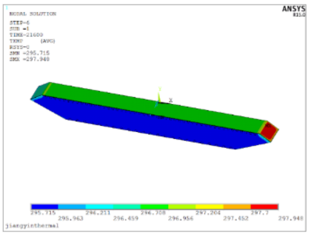
(b) 6:00

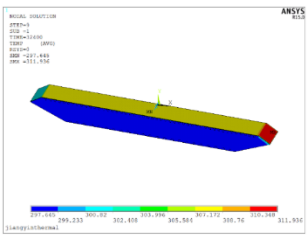
(c) 9:00

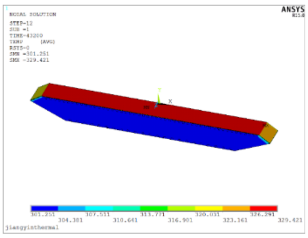
(d) 12:00

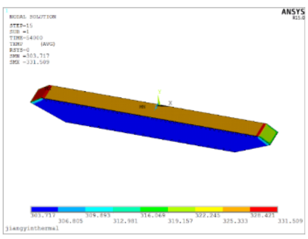
(e) 15:00

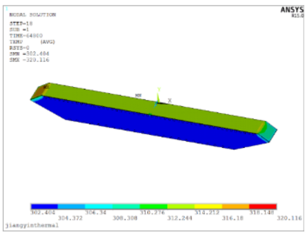
(f) 18:00

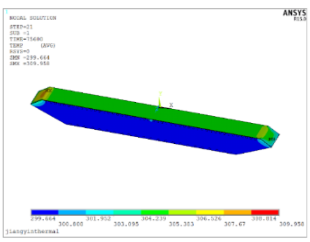
(g) 21:00

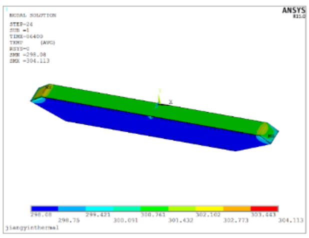
(h) 24:00

Fig. 13 Temperature fields of box girder on June 13, 2006, temperature distribution (°K)

When modified turbidity coefficients are calculated from the temperature difference between the north and south anchors, and brought into equations 1~8 to accurately solve the solar radiation density. And then, a modified solar radiation model can be established and used into a reliable FEM to perform the temperature prediction.

4.2 Temperature variation of the box-girder section

A typical sunny day such as June 13, 2006, which featured relatively high solar radiation and air temperature, is selected for the simulation. The wind speed of the day is less than 1 m/s. The solar radiation densities of the top deck and web are calculated with the modified formulas, and are shown in Fig. 12, where the top deck of the box girder receives the largest amount of solar radiation, reaching a maximum of 852 W/m^2 at 12:00. The downstream web begins to receive solar radiation at 6:00, and reaches its maximum at 11:00. The upstream web begins to receive solar radiation at 8:00, and reaches the maximum at 13:00.

The calculated total solar radiation energy and boundary conditions are brought into the FEM for the transient temperature field analysis. The simulation results at different time as shown in Fig. 13. The temperature in the Fig. 13 indicates the Kelvin temperature. When the sun rises, the downstream web is the first solar radiation received and the temperature rises fastest, as shown in Fig. 13(c). And then, the temperature of upper deck starts to rise, and the temperature reaches the maximum value at 15:00 as shown in Figs. 13(d)-(e). The maximum temperature of upstream web appears later than the values of upper deck and downstream web. After the sun goes down, the temperature of the structure begins to drop because the structure emits thermal radiation to the surroundings. Detailed simulation and measured values are compared as follows.

The simulation results with different models (the modified model with γ and traditional model with different $t_u = 2, 4, 6$) are now compared. The comparison results between the finite-element simulation and the measured temperature are shown in Fig. 14. Fig. 14(a) shows temperature variations at upper deck. From the time of 0:00~6:00, the temperature of upper deck shows a decrease due to the decrease of ambient temperature. The results of all simulations and measurements are the same because there is no influence of solar radiation at that time. From the time of 7:00~15:00, the temperature of the upper deck continues to rise and reach maximum because of the increase in solar radiation. It can be observed that the simulated temperature with modified model is in good agreement with the actual measurements. But the results with different values of $t_u = 2, 4, 6$ are not consistent with the actual measurements, especially for $t_u = 2$. So, the different turbidity coefficients t_u which depends on human judgment directly lead to inaccurate simulation results of the structure temperature. From the time of 16:00~24:00, The temperature of upper deck begins to decrease because of the weakening of solar radiation. The Fig. 14(b) shows temperature variations at lower deck. The predicted temperatures with the modified model and traditional model

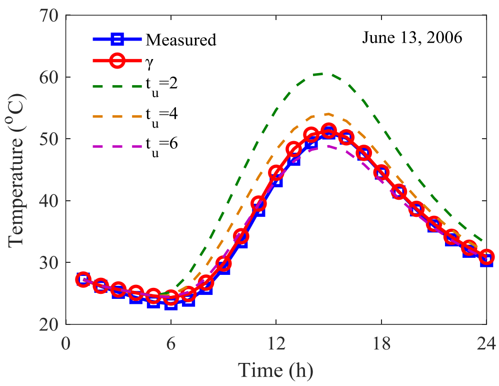

(a) On the topper deck

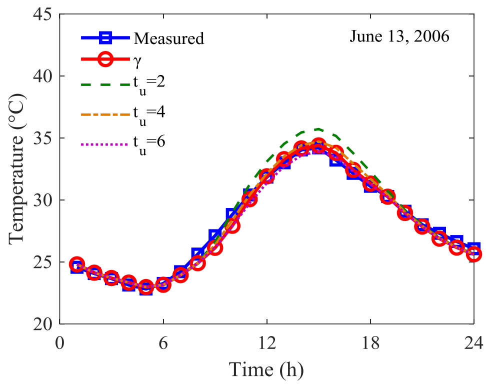

(b) On the lower deck

Fig. 14 Measured and simulated temperatures of box girder on June 13, 2006

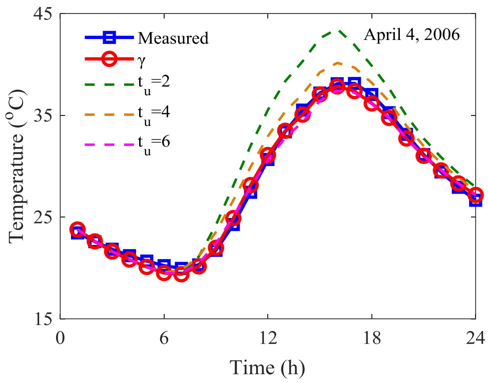

(a) On the topper deck

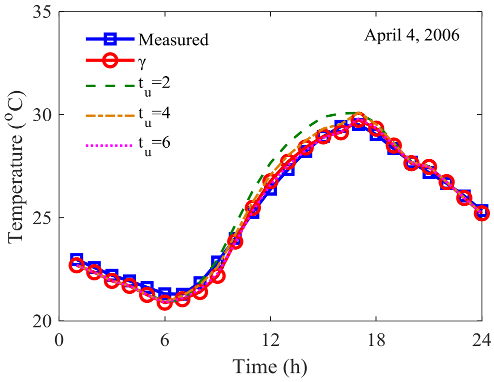

(b) On the lower deck

Fig. 15 Measured and simulated temperatures of box girder on April 4, 2006

are consistent with the actual temperatures. Because of the temperature of lower deck is not exposed to direct sunlight and mainly depend on the effects of heat conduction and ambient temperature.

A sunny day of April 4, 2006 are selected for thermal analysis. The comparisons between the simulated and the measured temperature are shown in Fig. 15. From the Fig. 15(a), the simulated temperatures with the different values of $t_u = 2, 4$, are not good agreement with the measured temperature. But the simulation results are very close to the actual measurements based on $t_u = 6$. It is undeniable that when the turbidity coefficient t_u takes a certain value, the simulation results are also satisfactory. However, this value is not known without performing multiple simulations and it takes more calculation time to determine. When using the proposed model with modified coefficient γ, the simulated temperature is in good agreement with the measured temperature, and the phenomenon of Fig. 15(b) is also the same to Fig 14(b).

4.3 Temperature gradient of the box girder

The temperature gradient induces thermal stress, thus it is an important parameter in the long-span bridge design. The temperature gradients of the box girder in both the vertical and transversal directions are investigated in day of June 13, 2006.

4.3.1 Vertical temperature gradient of the box girder

When the temperature distribution of the cross section is accurately simulated, the temperature gradient distribution can be determined. Fig. 16(a) shows the temperature gradient of the cross-section at mid-sapn, with the z-axis representing the height of the section, the y-axis representing the time, and the x-axis representing the temperature. During the day, the highest temperatures of the top and bottom decks reach up to 49°C and 34°C, respectively. The highest temperature occurs at 13:00, at this time, the temperature envelope line represents the temperature gradient of the cross-section, as shown in Fig. 16(a). As shown in Fig. 16(b), the temperature gradient in the vertical direction of the mid-span cross section is calculated from the monitoring data. It is seen that the measured values are slightly smaller than that those defined in design codes.

4.3.2 Transverse temperature gradient of the box girder

The analyses of transversal temperature gradient are as follow. Fig. 17(a) shows the transverse temperature of the top deck, where the 3D surface represents the temperature variations during the day, and the projection at the bottom represents the temperature distribution at each moment. It is observed that the transverse temperature difference is

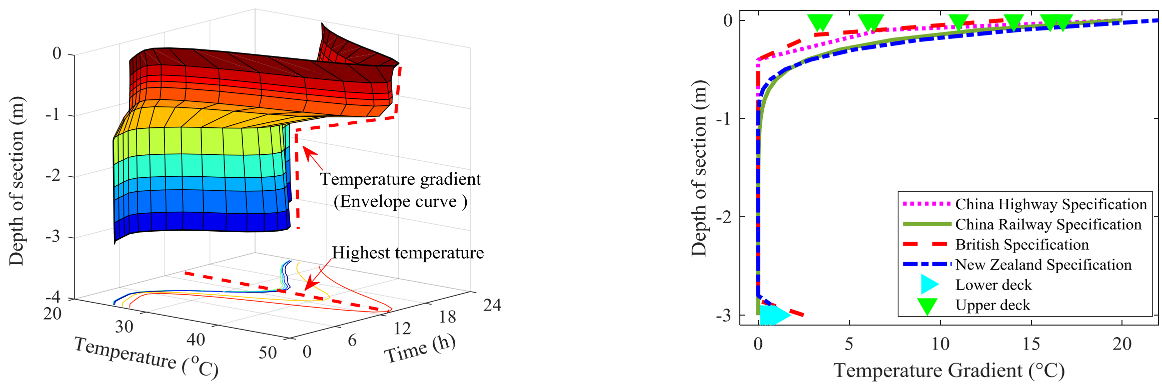

(a) Simulated gradient (b) Measured gradient

Fig. 16 Vertical temperature gradient

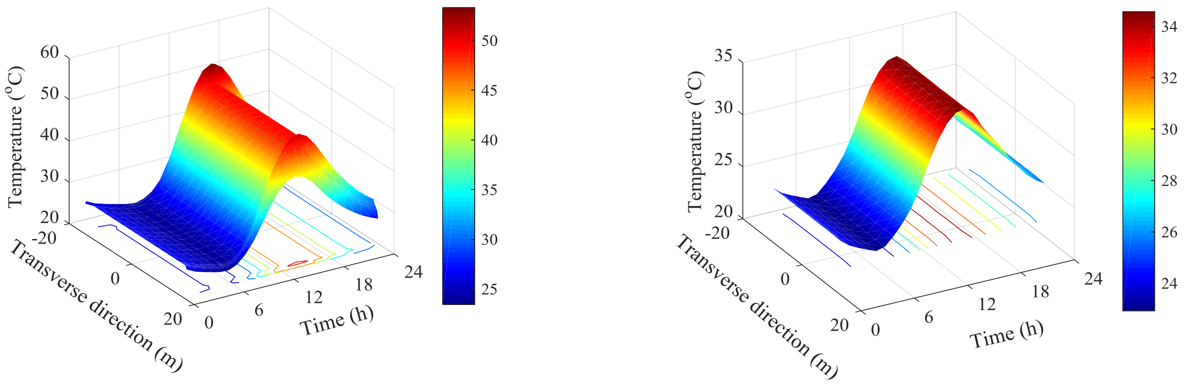

(a) On the upper deck (b) On the lower deck

Fig. 17 Transverse temperature gradient

relatively small, but the temperature difference between the top and the web is greater than that at the other positions. Fig. 17(b) shows the transverse distribution of the bottom deck of the box girder, where there is little temperature difference in the transverse temperature distribution of the bottom deck, because of the lack of direct solar radiation from the sun.

5. Thermal analysis of the bridge tower

5.1 Tower segment model

The height of the north and south bridge towers is 190 m, which consist of two reinforced concrete hollow columns and three horizontal beams, with a concrete thickness of 2 m, resulting in a greater temperature difference between the inside and outside of the tower under the effect of solar insolation. A detailed FEM of one tower segment is constructed using 1,051,267 nodes and 248,400 three-dimensional solid elements (solid 90) as shown in Fig. 18(a). The solar intensity on the tower surfaces differs from that on the deck surface, with different facades receiving different levels of solar radiation. First, detailed physical parameters of each surface of the tower were calculated as shown in Table 4. Second, Fig. 18(b) shows the solar radiation intensity on each surface on June

Table 4 Geography parameters for tower

Parameters	Value
Latitude	31.94°
Dip angle(A1-A6)	90°
Sun declination angle	-14.59°
Surface azimuth angle (A1)	24.40°
Surface azimuth angle (A2)	100.36°
Surface azimuth angle (A3)	128.43°
Surface azimuth angle (A4)	-155.60°
Surface azimuth angle (A5)	-79.64°
Surface azimuth angle (A6)	-51.57°

13, 2006 calculated with the modified formula, which indicates a peak solar intensity at about 09:00 on the eastern surface and about 16:00 h on the western surface.

5.2 Temperature distribution of the bridge tower

The variation in temperature at the tower section on June 13, 2006 was calculated and shown in Fig. 19. Only the numerical results are reported here because no temperature sensor is installed on the tower. Fig. 19 shows the temperature variation of each surface of the bridge

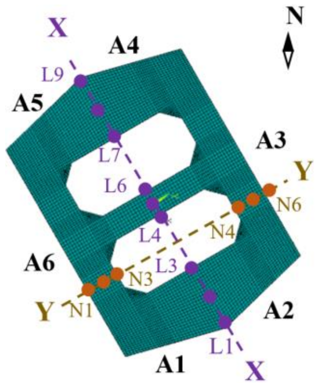

(a) Tower segment model

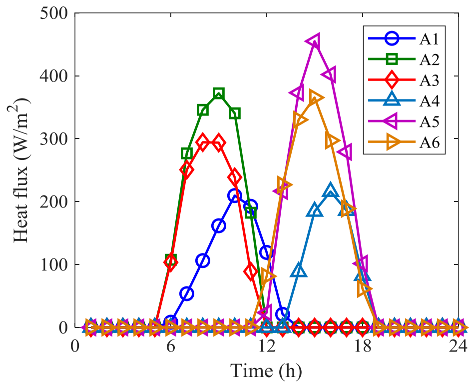

(b) Solar radiation intensity on each surface

Fig. 18 The FEM of the bridge tower

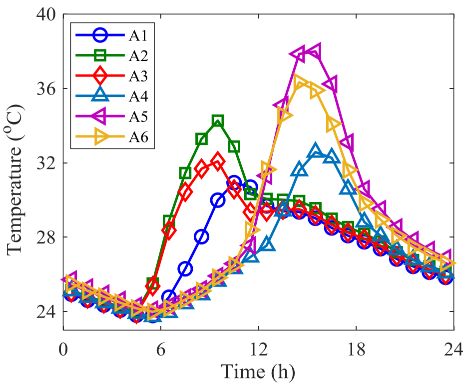

Fig. 19 Temperature variation on each surface

tower. As each of these surfaces has a different orientation, each receives a large difference in the solar radiation intensity as shown in Fig. 18(b). The surfaces A1, A2, A3 receive the direct radiation of the sun in the morning, reaching the maximum at 10:00. The surfaces A4, A5, A6 receive the direct radiation of the sun in the afternoon, reaching the maximum at 16:00.

The temperatures in the X- and Y-directions of the cross-section of the tower are extracted from the points shown in Fig. 18(a), and used to study the temperature change inside the bridge tower. Fig. 20 shows the X- and Y-directions of the temperature changes, with the distribution of the temperature field in the X-X direction shown in Fig. 20(a). The temperature of the outer surface of the bridge tower varies from 24°C to 38°C during the day, with the temperature change inside the tower very small, and not exceeding 2°C. The distribution of temperature field in the Y-Y direction is shown in Fig. 20(b), with the temperature change in the Y-direction of the bridge tower similar to the temperature change in the X-direction. As the bridge is a concrete structure, with very thick, poor thermal conductivity, this gives a large temperature difference between the interior and exterior of the bridge tower. Therefore, the thermal stress of the bridge tower should be closely considered in practical engineering applications.

6. Conclusions

In this article, the authors studied the temperature monitoring data which was influenced by the solar radiation and seasonal temperature changes to find that the temperature difference can be used to describe the real-time weather changes. As the traditional calculation of solar radiation intensity does not consider the effects of time-varying weather, the authors established a time-varying solar radiation model based on the temperature difference of the north and south anchors. The temperature distribution of

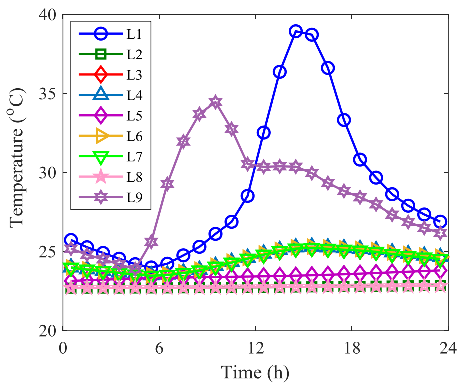

(a) X-X section

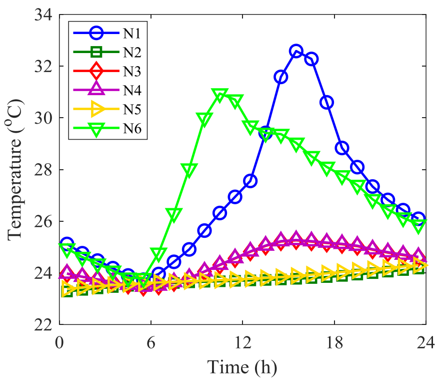

(b) Y-Y section

Fig. 20 Variation in temperature at the tower section typical box-girder and tower sections are studied by using the modified solar-radiation model.

The following conclusions can be drawn:

- By analyzing the temperature data of the south and the north anchors, the temperature difference is attributable to the additional heating caused by direct solar radiation, which reflects the change in the real-time weather conditions. The time-varying coefficient was established based on the temperature difference which enable the traditional solar-radiation model to fully consider the effects of weather changes in real-time.
- A transient heat-transfer analysis based on the modified solar radiation model is carried out to show that the temperature field calculated by the modified model is in good agreement with the measured temperature. At the same time, the temperature field calculated on the traditional solar-radiation model shows a minor error, especially on the top deck. Furthermore, the vertical and transverse temperature gradient of a typical box girder is simulated and analyzed.
- Although the studied bridge towers are not equipped with temperature sensors, the temperature distribution of the tower is also studied. The results show that a large temperature difference between the interior and exterior of the bridge tower. The thermal stress of the bridge tower should be considered in practical engineering.

Acknowledgments

The research presented was financially supported by the National Key R&D Program of China (No.: 2018YFC0705601), Jiangsu Distinguished Young Scholars Fund (No.: BK20160002) and National Science Foundation of China (Grant No.: 51578139, 51778134).

References

Abid, S.R., Mussa, F., Tayşi, N. and Özakça, M. (2018), "Experimental and finite element investigation of temperature distributions in concrete-encased steel girders", *Struct. Control Health Monit*., **25**(1), 1:23. https://doi.org/10.1002/stc.2042

ANSYS 15 [Computer software]. Southpointe, PA, ANSYS.

Branco, F.A. and Mendes, P.A. (1993), "Thermal actions for concrete bridge design", *J. Struct. Eng.*, **119**(8), 2313-2331. https://doi.org/10.1061/(ASCE)07339445(1993)119:8(2313)

Chen, B., Chen, Z.W., Sun, Y.Z. and Zhao, S.L. (2013), "Condition assessment on thermal effects of a suspension bridge based on SHM oriented model and data", *Math. Probl. Eng.*, 1-18. http://dx.doi.org/10.1155/2013/256816

Chen, C.C., Wu, W.H., Liu, C.Y. and Lai, G.L. (2017), "Elimination of environmental temperature effect form the variation of stay cable force based on simple temperature measurements", *Smart Struct. Syst., Int. J.*, **19**(2), 137-149. https://doi.org/10.12989/sss.2017.19.2.137

Dilger, W.H., Ghali, A., Chan, M., Cheung, M.S. and Maes, M.A. (1983), "Temperature stresses in composite box girder bridges", *J. Struct. Eng.*, **109**(6), 1460-1478. https://doi.org/10.1061/(ASCE)0733-9445(1983)109:6(1460)

Elbadry, M.M. and Ghali, A. (1983), "Temperature variation in concrete bridges", *J. Struct. Eng.*, **109**(10), 2355-2374. https://doi.org/10.1061/(ASCE)0733-9445(1983)109:10(2355)

Kim, S.H., Cho, K.I., Won, J.H. and Kim, J.H. (2009), "A study on thermal behaviour of curved steel box girder bridges considering solar radiation", *Arch. Civil Mech. Eng.*, **9**(3), 59-76. https://doi.org/10.1016/S1644-9665(12)60218-0

Kim, H.Y., Kang, D.H and Kim, D.H. (2017), "Mechanical strength of FBG sensor exposed to cyclic thermal load for structural health monitoring", *Smart Struct. Syst., Int. J.*, **19**(3), 335-340. https://doi.org/10.12989/sss.2017.19.3.335

Ko, J.M. and Ni, Y.Q. (2005), "Technology developments in structural health monitoring of large-scale bridges", *Eng. Struct.*, **27**(12), 1715-1725. https://doi.org/10.1016/j.engstruct.2005.02.021

Li, S.S. (1996), *Physics of Solar Energy*, Capital Normal University Press, Beijing, China.

Liu, H.B., Chen, Z.H. and Zhou, T. (2012), "Theoretical and Experimental Study on the Temperature Distribution of H-Shaped Steel Members under Solar Radiation", *Appl. Thermal Eng.*. **37**, 329-335. https://doi.org/10.1016/j.applthermaleng.2011.11.045

Niu, Y.W., Zhao, Y., Qu, X.X., Yu, Q. and Huang, P.M. (2014), "The research of space temperature distribution in solid tower of extradosed cable-stayed bridge", *Open Constr. Build. Technol. J.*, **8**, 488-495. https://doi.org/10.2174/1874836801408010488

Rohsenow, W.M., Hartnett, J.P. and Cho, Y.I. (1998), *Handbook of Heat Transfer Applications*, (Third Edition), McGraw-Hill, New York, NY, USA.

Song, X.M., Melhem, H., Li, J., Xu, Q.Y. and Cheng, L.J. (2016), "Effects of solar temperature gradient on long-span concrete box girder during cantilever construction", *J. Bridge Eng.*, **21**(3), 04015061. https://doi.org/10.1061/(ASCE)BE.1943-5592.0000844

Threlkeld, J.L. (1970), *Thermal Environmental Engineering*, Prentice-Hall Inc., Englewood Cliffs, NJ, USA.

Tian, Y., Zhang, N. and Xia, H. (2017), "Temperature effect on service performance of high-speed railway concrete bridges", *Adv. Struct. Eng.*, **20**(6) 865-883. https://doi.org/10.1177/1369433216665306

Tong, M., Tham, L.G., Au, F.T.K. and Lee, P.K.K. (2001), "Numerical modeling for temperature distribution in steel bridges", *Comput. Struct.*, **79**(6), 583-593. https://doi.org/10.1016/S0045-7949(00)00161-9

Wang, Y.B., Zhan, Y.L. and Zhao, R.D. (2016), "Analysis of thermal behavior on concrete box-girder arch bridges under convection and solar radiation", *Adv. Struct. Eng.*, **19**(7), 1043-1059. https://doi.org/10.1177/1369433216630829

Westgate, R., Koo, K.Y. and Brownjohn, J. (2015), "Effect of solar radiation on suspension bridge performance", *J. Bridge Eng.*, **20**(5), 04014077. https://doi.org/10.1061/(ASCE)BE.1943-5592.0000668

Xia, Y., Chen, B., Zhou, X.Q. and Xu, Y.L. (2013), "Field monitoring and numerical analysis of tsing ma suspension bridge temperature behavior", *Struct. Control Health Monit.*, **20**(4), 560-575. https://doi.org/10.1002/stc.515

Xia, Q., Cheng, Y.Y., Zhang, J. and Zhu, F.Q. (2017a), "In-service condition assessment of a long-span suspension bridge using temperature-induced strain data", *J. Bridge Eng.*, **22**(3), 04016124. https://doi.org/10.1061/(ASCE)BE.1943-5592.0001003

Xia, Q., Zhang, J., Tian, Y. and Zhang, Y.F. (2017b), "Experimental study of thermal effects on a long-span suspension bridge", *J. Bridge Eng.*, **22**(7), 04017034. https://doi.org/10.1061/(ASCE)BE.1943-5592.0001083

Xu, Y.L., Chen, B., Ng, C.L., Wong, K.Y. and Chan, W.Y. (2010), "Monitoring temperature effect on a long suspension bridge", *Struct. Control Health Monit.*, **17**(6), 632-653. https://doi.org/10.1002/stc.340

Yang, X., Zhang, J. and Ren, W.X. (2017), "Temperature effect analysis of a long-span cable-stayed bridge based on extreme strain estimation", *Smart Struct. Syst., Int. J.*, **20**(1), 11-22. https://doi.org/10.12989/sss.2017.20.1.011

Zhang, J., Wan, C.F. and Sato, T. (2013), "Advanced markov chain monte carlo approach for finite element calibration under uncertainty", *Computer-Aided Civil Infrastruct. Eng.*, **28**(7), 522-530. https://doi.org/10.1111/j.1467-8667.2012.00802.x

Zhou, G.D. and Yi, T.H. (2013), "Thermal load large-scale bridges: a state-of-the-art review", *Int. J. Distrib. Sensor Networks*, **9**(12), 1-17. https://doi.org/10.1155/2013/217983

Zhou, Y., Sun, L.M. and Peng, Z.J. (2015), "Mechanisms of thermally induced deflection of a long-span cable-stayed bridge", *Smart Struct. Syst., Int. J.*, **15**(3), 505-522. http://dx.doi.org/10.12989/sss.2015.15.3.505

Zhou, L.R., Xia, Y., Brownjohn, J.M.W. and Koo, K.Y. (2016), "Temperature analysis of a long-Span suspension bridge based on field monitoring and numerical simulation", *J. Bridge Eng.*, **21**(1), 04015027. https://doi.org/10.1061/(ASCE)BE.1943-5592.0000786

Zhu, J.S. and Meng, Q.L. (2017), "Effective and fine analysis for temperature effect of bridges in natural environments", *J. Bridge Eng.*, **22**(6), 04017017. https://doi.org/10.1061/(ASCE)BE.1943-5592.0001039

CC